Floating Random Walk-Based Capacitance Extraction for General Non-Manhattan Conductor Structures

Zhezhao Xu, Chao Zhang, and Wenjian Yu, *Senior Member, IEEE*

***Abstract*—The non-Manhattan conductor geometry existing in some capacitance extraction problems brings difficulty to the floating random walk (FRW) method using cubic transition domains. In this paper, techniques are proposed to enhance the FRW method for handling the structures with non-Manhattan conductors. Based on the aligned-box distances and corresponding calculating approaches, the techniques for generating the Gaussian surface and constructing axis-aligned transition cubes are proposed. A practical strategy is then proposed to judge the domination relationship of non-Manhattan conductor blocks for building the space management structure with candidate list. Finally, the strategy using rotated transition cube and related space management technique are proposed to make further acceleration. Experiments on 3-D interconnect structures including from 8 to 1000 non-Manhattan blocks show that the proposed method is from 2.9× to 96× faster than a simple extension of the original FRW method. The proposed method is also up to 39× faster than a boundary element method-based solver. Additional experiments are carried out to further validate the accuracy and efficiency of the proposed techniques, and to demonstrate their suitability for large and multi-dielectric structures.**

***Index Terms*—Capacitance extraction, domination relationship judgement, floating random walk (FRW) method, non-Manhattan geometry, nearest neighbors algorithm, space management.**

I. Introduction

THE CAPACITANCE extraction problem arose in the design of integrated circuits (ICs) under deep submicron process technology. With the increase of the devices integrated in a single IC chip, the parasitic effect of interconnects greatly degrades the circuit performance and leads to signal integrity and power integrity problems. Although the parasitic effect can be accurately modeled with comprehensive electromagnetic simulations, in many scenarios the resistance and capacitance models are sufficient and practical for reducing the computational cost [1]. The capacitance extraction, in which the capacitance model for the interconnects is built with various numerical approaches, has become a key step in IC design. It is the basis of accurate circuit simulation and physical verification for quality IC design. The capacitance extraction is also required in other electronic design problems, e.g., the design of flat panel display (FPD) [2]. To verify that the signal delay to all display pixels has zero skew, the capacitances of FPD wires should be accurately calculated. The design of touch panel, a special kind of FPD, also requests accurate capacitance calculation for verifying the performance of capacitive location sensors.

Having been studied for three decades, the capacitance extraction is still faced with challenges. A major challenge is associated with large-scale and complicated structure, which greatly reduces the accuracy and efficiency of capacitance extraction. The emerging device and interconnect technologies in nanometer ICs have made the structure of interconnects in digital circuits more complex [3]. As for analog/RF IC, package, and FPD designs, the wire and conductor structures therein exhibit more complexity in geometry. On the other hand, with decreased performance margin, more accuracy on capacitance extraction is demanded in order to keep a reasonable yield. Therefore, high-precision capacitance extraction for large-scale and complicated structures is very desirable.

A lot of field-solver techniques, which accurately simulate the electrostatic field around conductors, have been proposed for the capacitance extraction. They can be classified into two categories: 1) the traditional deterministic methods [4]–[9] and 2) the floating random walk (FRW) method [10]–[20]. Some of them, like FastCap [4], QBEM [5], RedCap [6] and the FRW-based techniques [10], [17], [20], have become the engines of commercial tools. The traditional methods require the volume or surface discretization of the problem domain and result in a system of linear equations. They include the fast boundary element methods (BEMs) [4]–[8], the parallel adaptive finite-element method [9], etc. These methods are fast, accurate and versatile, but not suitable for large-scale structures due to the large demand of computational time and the bottleneck of memory usage. On the contrary, the FRW method is a kind of Monte Carlo (MC) method. Therefore, it has the advantages of better scalability for very large structures, tunable accuracy, better parallelism, and much smaller memory usage [13]–[15]. A recent work on structures with large cylindrical through-silicon vias (TSVs) [19] revealed

Manuscript received November 26, 2015; revised February 20, 2016 and April 14, 2016; accepted April 28, 2016. Date of publication May 3, 2016; date of current version December 20, 2016. This work was supported by the National Natural Science Foundation of China Research Project under Grant 61422402. This paper was recommended by Associate Editor H. Qian. *(Zhezhao Xu and Chao Zhang contributed equally to this work.) (Corresponding author: Wenjian Yu.)*

The authors are with the Tsinghua National Laboratory for Information Science and Technology, Department of Computer Science and Technology, Tsinghua University, Beijing 100084, China (e-mail: yu-wj@tsinghua.edu.cn).

Color versions of one or more of the figures in this paper are available online at http://ieeexplore.ieee.org.

Digital Object Identifier 10.1109/TCAD.2016.2561968

that, the accuracy of the BEM-based capacitance solver (especially on coupling capacitance) is susceptible to the boundary discretization scheme, and could be much worse than that of the FRW method. So, the latter can be considered to be more reliable on accuracy than the BEM solvers.

With the advent of multiprocessor and parallel computing techniques [21], [22], the FRW method has become popular and been applied to the block- or chip-level extraction in the sign-off verification of digital ICs [15], [20]. However, the FRW method and relevant techniques [10]–[15], [17], [20] for capacitance extraction, including the employment of axis-aligned (Manhattan) cubic transition domains and relevant techniques for multi-dielectric per-characterization, space management, and etc., depend on the assumption that the handled geometries are all of Manhattan shape. To handle non-Manhattan geometry, Manhattan geometry approximation is applied in some commercial tools, which, however, results in loss of accuracy or even an error [23]. The assumption of Manhattan geometry is basically true for digital ICs, where the conductor and dielectric interfaces are either parallel or perpendicular to one another. However, it is not true for the structures in analog/RF circuit, packaging structure, or FPD design, where there are considerable bevel metal wires and general nonrectangular conductor shapes. With the increase of device density, the design of analog, mixed-signal circuit, or packaging structure also requires the FRW-like technique for accurate capacitance extraction. So, the extension of the FRW method for general non-Manhattan geometries becomes important.

There is little research devoted to the FRW method for extracting the capacitances of general geometries. In [16], an FRW method using spherical transition domains, also known as the walk on sphere (WOS) method [24], was presented for the capacitance extraction of general geometries. However, it was restricted to single-dielectric structures, and did not include any accelerating technique. Recently, an improvement of the method in [16] was proposed for 2-D non-Manhattan geometries, which facilitates the construction of transition spheres with a distance map [18]. However, generating the distance map with sufficient resolution needs considerable computational cost. Therefore, the method is not efficient for actual 3-D large-scale structures. Fast FRW-based techniques for handling cylindrical intertier-vias in 3-D IC have been proposed in [19], where only the non-Manhattan object of cylinder shape is considered. Thus, the techniques in [19] are not suitable for the general non-Manhattan structures in analog circuit, package or FPD.

In this paper, we develop the FRW-based techniques for capacitance extraction of general non-Manhattan conductor structures. Because the flattening process, like the chemical-mechanical polishing, is applied in the manufacture of ICs and FPD devices, the non-Manhattan conductor considered in this paper can be regarded as a straight prism with arbitrary polygon as the bottom. For a structure including both these non-Manhattan conductors and Manhattan rectangular conductors, the techniques for generating the Gaussian surface and efficiently performing FRWs are proposed. They extend the conventional FRW method only suitable for Manhattan geometry, and enable efficient FRW-based capacitance extraction for the large-scale non-Manhattan conductor structures. Numerical experiments with typical 3-D conductor structures in mixed-signal circuits and packaging components have validated the accuracy and the efficiency of the proposed techniques. Compared with a space management approach using an additional grid structure, the proposed technique makes faster random walk procedure and consumes much less memory. The comparison with fast BEM-based capacitance solver also demonstrates several tens times speedup and huge memory saving of the proposed FRW method. Further experiments are carried out to validate the accuracy and efficiency of the proposed techniques, and to demonstrate their suitability for large and multi-dielectric structures.

The main contributions of this paper are as follows.

1) It is the first random walk method using cubic transition domains for extracting the capacitances of general non-Manhattan conductors with polygon cross section.
2) By defining the distances related to the non-Manhattan conductor geometry and deriving their calculating formulas, we propose the techniques for generating the Gaussian surface and constructing the axis-aligned or rotated transition cube. They enable the accurate FRW algorithm for extracting the capacitances of non-Manhattan structures.
3) Through utilizing the sufficient conditions for domination, and the concepts of the domination of a block set and strong domination, efficient techniques are proposed for judging the domination of non-Manhattan conductor and constructing the space management structure with the candidate list. This space management technique achieves up to 84× speedup for a structure with 1240 non-Manhattan conductor blocks.
4) Combining the strategy of rotating the transition cube and the modified space management, the proposed FRW solver is up to 96× faster than the simply extended FRW algorithm for the non-Manhattan structures, without loss of accuracy.

The rest of this paper is organized as follows. The background of the FRW algorithm for the capacitance extraction with Manhattan conductors and related space management technique for large-scale problems are briefly introduced in Section II. The main contributions of this paper are presented in Section III, including the technique for generating the Gaussian surface, the FRW algorithm with axis-aligned transition cube and related space management techniques, and the FRW algorithm using rotated transition cube and modified space management techniques. In Section IV, some test cases with non-Manhattan conductors from mixed-signal circuits and packaging structures are extracted with the proposed FRW method. The numerical results are also compared with those obtained with a fast BEM solver. Finally, we draw the conclusions.

II. Background

A. FRW Algorithm for 3-D Capacitance Extraction

The FRW method for calculating electrostatic capacitance is originated from expressing the electric potential of a point $\boldsymbol{r}$ as

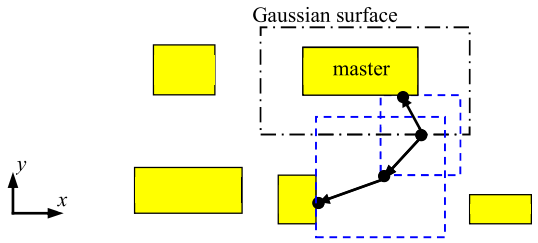

Fig. 1. Two examples of random walk in the FRW method for capacitance extraction (a 2-D top view).

an integral of the potential on surface S enclosing $\boldsymbol{r}$ [10], [11]

$$\phi(\boldsymbol{r}) = \oint_S P(\boldsymbol{r}, \boldsymbol{r}^{(1)})\phi(\boldsymbol{r}^{(1)})\mathrm{d}\boldsymbol{r}^{(1)} \tag{1}$$

where $P(\boldsymbol{r}, \boldsymbol{r}^{(1)})$ is called surface Green's function and can be regarded as a probability density function with non-negative value. Therefore, $\phi(\boldsymbol{r})$ is the statistical mean of $\phi(\boldsymbol{r}^{(1)})$, and can be calculated with an MC procedure sampling S. The domain enclosed by S is called transition domain, and usually $\boldsymbol{r}$ is the center of the transition domain.

The problem of capacitance extraction is to calculate the capacitances related to a specified conductor (called master conductor). For master conductor i, a Gaussian surface G_i is constructed to enclose it (see Fig. 1). According to the Gauss theorem, the charge of conductor i

$$Q_i = \oint_{G_i} F(\boldsymbol{r})g \int_{S^{(1)}} \omega(\boldsymbol{r}, \boldsymbol{r}^{(1)})q(\boldsymbol{r}, \boldsymbol{r}^{(1)})\phi(\boldsymbol{r}^{(1)})\mathrm{d}\boldsymbol{r}^{(1)}\mathrm{d}\boldsymbol{r} \tag{2}$$

where $F(\boldsymbol{r})$ is the dielectric permittivity at point $\boldsymbol{r}$, $q(\boldsymbol{r}, \boldsymbol{r}^{(1)})$ is the probability density function for sampling on $S^{(1)}$, the surface of a transition domain. g is a constant, which satisfies $\oint_{G_i} F(\boldsymbol{r})g\mathrm{d}\boldsymbol{r} = 1$. $q(\boldsymbol{r}, \boldsymbol{r}^{(1)})$ may be different from $P(\boldsymbol{r}, \boldsymbol{r}^{(1)})$, and $\omega(\boldsymbol{r}, \boldsymbol{r}^{(1)})$ is the weight value [11]. Thus, Q_i can be estimated as the statistical mean of sampled values on G_i, which is further the mean of sampled potentials on $S^{(1)}$ multiplying the weight value. If the sampled potential is unknown, the construction of transition domain and the spatial sampling procedure will repeat until a point with known potential is obtained (e.g., on conductor surface). This forms an FRW including a sequence of hops. Each hop is from the center of a transition domain to its boundary. With a number of such walks, the statistical mean of the weight values for the walks terminating at conductor j approximates the capacitance C_{ij} between conductors i and j (if $j \neq i$), or the self-capacitance C_{ii} of master conductor i.

Although the surface Green's function for a spherical transition domain has simple analytical expression, the cubic transition domain is widely adopted because it well fits the IC layout including mostly Manhattan shapes [10]–[13], [20]. This means larger probability for terminating a walk quickly. The sampling probability and weigh value for a cubic domain can be precalculated and tabulated, so as to accelerate the sampling operation.

The runtime of the FRW method is proportional to the number of random walks. Several variance reduction techniques has been proposed to reduce the number of walks [11], [19], i.e., accelerate the convergence of MC procedure. A walk consists of a couple of hops. For a structure including many conductors, employing an efficient space management technique is crucial for reducing the time for performing a hop.

B. Space Management Techniques for Manhattan Structure

A major step in each FRW hop is constructing a conductor-free transition cube (see Fig. 1). To be efficient, the cube should be as large as possible. This asks for finding the nearest conductor. Its distance from the current walk position is half of the transition cube's size. Since millions of hops are performed, this distance should be calculated as fast as possible. The idea of space management is to divide the whole 3-D domain into organized small subdomains (called spatial cell). By storing the information of neighboring conductors for a cell, we can quickly calculate the distance to the nearest conductor for any point in the cell.

The space management techniques have been investigated for structures including only Manhattan conductors [11], [12], [17], [20]. Here, "Manhattan" refers to a shape or shapes with each surface parallel to one of the *xoy*, *yoz*, and *zox* axis planes. A major idea is to maintain a candidate list of conductor cuboids for each spatial cell, such that for any point in the cell its nearest conductor is in the list. Therefore, the inquiry of nearest conductor only demands to traverse the candidate list and can be executed very quickly.

Two steps of the space management are constructing the spatial structure and inquiring the nearest conductor with it. The former has some runtime and memory cost, while the latter reduces the runtime of random walk. The octree and grid are two widely-used spatial structures to organize the spatial cells. In [12], a grid-octree hybrid structure was proposed, and shown to be superior to other structures in terms of the time for performing random walks and the memory overhead.

In constructing the spatial structure, a primary operation is generating the candidate list for a cell. We shall check the conductor cuboids one by one to see if they should be added to the list. During this course, the domination relationship between two conductor cuboids is considered.

Definition 1: T is a spatial cell, and B_1, B_2 are two conductor cuboids. If for any point $\boldsymbol{P} \in T$, and $\boldsymbol{P} \notin B_1 \cup B_2$, $d(\boldsymbol{P}, B_1) \leq d(\boldsymbol{P}, B_2)$, we say B_1 *dominates* B_2 regarding T.

If B_1 dominates B_2 regarding cell T, and B_1 is already in T's candidate list, B_2 should not be inserted to the list. Here $d(,)$ denotes the distance between a point and a cuboid, which is actually the half size of the Manhattan (axis-aligned) cube centered at the point and touching the cuboid. This distance is very similar to the ∞-norm distance, but allows negative value. We call it the *aligned-box distance*. Similar distance was defined between two Manhattan cuboids [12].

With a distance limit $L(T)$, the upper bound of the distance to nearest block from points in cell T, a pruning technique was proposed in [12] to largely reduce the time for generating the candidate lists and the space management structure. The procedure checking if conductor B should be added to the candidate list of T is described as Algorithm 1.

Algorithm 1 CandidateCheck (conductor B, cell T)

```
1: d := d(B, T); l is the size of T;
2: If d ≥ L(T) then return false;
3: For each b in the candidate list of T do
4:    If b dominates B then return false;
5:    Elseif B dominates b then
6:       Remove b from the candidate list of T;
7:    Endif
8: Endfor
9: Add B to the candidate list of T;
10: If (d + l) < L(T) then L(T) := d + l;
11: return true.
```

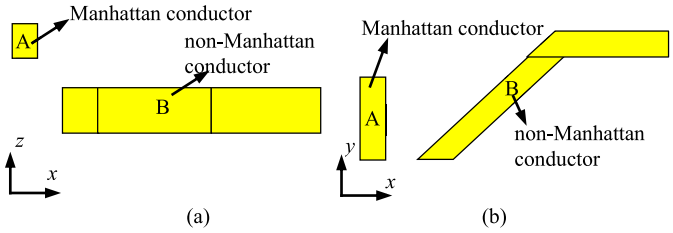

Fig. 2. Manhattan conductor (A) and a non-Manhattan conductor (B) in IC layout. (a) Side view (on the zox plane). (b) Top view (on the xoy plane).

It should be pointed out that judging the domination relationship is not difficult for two Manhattan cuboids. However, if one of the conductor is of non-Manhattan shape, it becomes difficult.

III. Efficient Techniques for Handling Non-Manhattan Conductors

In this section, we first introduce the assumptions for the considered capacitance extraction problem and establish the basic distance calculation technique. Then, the technique for generating the Gaussian surface is proposed. In the last two sections, the FRW algorithms using Manhattan transition cube and rotated transition cubes are proposed, respectively, with the focus on efficient space management techniques for handling a considerable number of non-Manhattan conductors.

A. Basic Considerations and Distance Calculation

In this paper, we refer to the non-Manhattan conductors as the bevel metal wires/conductors in IC layout or FPD layout. The 3-D geometry of this kind of conductor has top and bottom faces parallel to the xoy-axis plane. However, its projection on the xoy plane (i.e., the top view) is an arbitrary 2-D polygon, instead of an axis-aligned rectangle. Without loss of generality, we assume that this 2-D polygon is always convex. Actually, a preprocess step is often employed before capacitance extraction to decompose complex conductor geometry into convex triangles and quadrangles (see Fig. 2).

Now, the problem includes a number of 3-D conductor blocks. Each block is either a Manhattan cuboid or a convex straight prism with side faces perpendicular to the xoy plane. The master conductor may include a couple of connected conductor blocks. While running capacitance extraction with the FRW algorithm, we only consider the cubic transition domain, since it well touches the surface of the conductor and brings faster termination of a random walk.

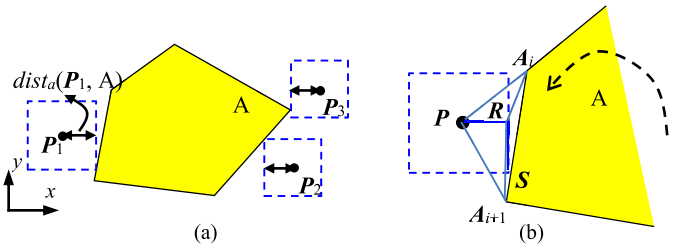

Fig. 3. Illustration of the 2-D aligned-box distance between a point and a polygon. (a) Aligned-box distances between A and three nearby points. (b) Illustration for the calculation of $\text{dist}_a(\boldsymbol{P}, A)$.

In the FRW algorithm, the distance calculation between a point and a block or between two blocks is required. If the block is of non-Manhattan shape, the calculation becomes complicated, bringing difficulty to the following parts of FRW algorithm.

1) The generation of the Gaussian surface, which must enclose the master conductor and not intersect any conductor.
2) The construction of the transition cube for each hop, which requests finding the nearest conductor for a point.
3) The space management which accelerates finding the nearest conductor for constructing the transition cube, especially useful for handling structure with a large number of blocks.

The aligned-box distance for Manhattan geometry should be extended for non-Manhattan geometry. For the problem considered in this paper, we define some basic distances.

Definition 2: The 2-D aligned-box distance between a 2-D point $\boldsymbol{P}$ and a convex polygon A: $\text{dist}_a(\boldsymbol{P}, A)$, is the half size of the axis-aligned square which is centered at $\boldsymbol{P}$ and touches A.

In Fig. 3(a), we show some typical positions of a point around polygon A. The Manhattan transition squares and the corresponding aligned-box distances are depicted. In Fig. 3(b), we show the basic idea for calculating $\text{dist}_a(\boldsymbol{P}, A)$. We first find the visible edges of A regarding to point $\boldsymbol{P}$. If the Manhattan square centered at $\boldsymbol{P}$ touches A's edge, the edge must be a visible edge. For each edge $\overrightarrow{\boldsymbol{A}_i\boldsymbol{A}_{i+1}}$ of A, we calculate the cross product of $\overrightarrow{\boldsymbol{A}_i\boldsymbol{P}}$ and $\overrightarrow{\boldsymbol{A}_i\boldsymbol{A}_{i+1}}$. If the result is a positive value, edge $\overrightarrow{\boldsymbol{A}_i\boldsymbol{A}_{i+1}}$ is visible, and we get the area of triangle $\boldsymbol{PA}_i\boldsymbol{A}_{i+1}$. As shown in Fig. 3(b), the area is useful for calculating the size of the transition square. Triangle $\boldsymbol{PA}_i\boldsymbol{A}_{i+1}$ can be regarded as the combination of four triangles: 1) $\boldsymbol{PA}_i\boldsymbol{R}$; 2) $\boldsymbol{PRA}_{i+1}$; 3) $\boldsymbol{RA}_i\boldsymbol{S}$; and 4) $\boldsymbol{RSA}_{i+1}$, where $\boldsymbol{S}$ is the touching point and $\boldsymbol{R}$ is a midpoint of transition square's edge. The four triangles all have the half size of the transition square as a bottom edge, while the corresponding heights form the x-distance and y-distance between points $\boldsymbol{A}_i$ and $\boldsymbol{A}_{i+1}$. So, the cross product of $\overrightarrow{\boldsymbol{A}_i\boldsymbol{P}}$ and $\overrightarrow{\boldsymbol{A}_i\boldsymbol{A}_{i+1}}$ over the sum of the x-distance and y-distance equals the half edge length. $\text{dist}_a(\boldsymbol{P}, A)$ is the maximum of such half edge length got from all visible edges, or corresponds to the situation where the Manhattan square touches A's vertex

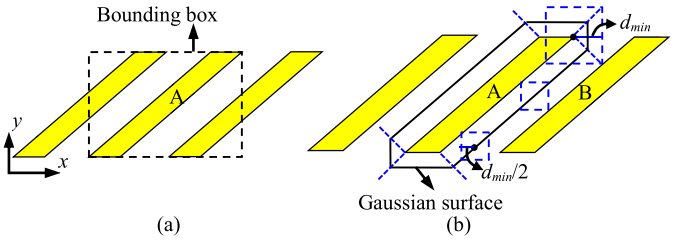

Fig. 4. Top view of a non-Manhattan conductor structure. (a) Master's bounding box. (b) Valid generation of the Gaussian surface.

[see $\boldsymbol{P}_3$'s square in Fig. 3(a)]. In the latter situation the distance can be obtained with the Manhattan bounding box of A, using existing technique. This analysis derives Theorem 1.

Theorem 1: Suppose polygon A has vertices $\boldsymbol{A}_1, \boldsymbol{A}_2, \ldots, \boldsymbol{A}_n$, in the anti-clockwise order. $\boldsymbol{A}_i$ has coordinates (x_i, y_i), $i = 1, 2, \ldots, n$. Suppose point $\boldsymbol{P}$ has coordinates (x, y). Then

$$\begin{aligned}&\text{dist}_a(\boldsymbol{P}, A)\\ &= \max\left\{\max_{1\le i\le n}\frac{(x-x_i)(y_{i+1}-y_i)-(y-y_i)(x_{i+1}-x_i)}{|x_{i+1}-x_i|+|y_{i+1}-y_i|}, \text{dist}_a(\boldsymbol{P}, B_A)\right\}\end{aligned} \tag{3}$$

where B_A is the Manhattan bounding box of polygon A. ■

The vertical distance between a point and a conductor block is defined as follows.

Definition 3: The vertical distance between a point $\boldsymbol{P}(x, y, z)$ and a non-Manhattan conductor block A is

$$\text{dist}_v(\boldsymbol{P}, A) = \max\{z - z_{\max}(A), z_{\min}(A) - z\} \tag{4}$$

where $z_{\min}(A)$ and $z_{\max}(A)$ are the minimum and maximum z coordinates of A, respectively.

B. Generation of Gaussian Surface

We first consider the situation where the master conductor only contains one block. In Fig. 4, the top view of a typical non-Manhattan structure is shown ("A" labels the master conductor). From Fig. 4(a), we see that the bounding box of the master intersects other conductor. Therefore, the strategy of generating the Gaussian surface for the Manhattan bounding box, which has been used for the cylindrical TSV [19], becomes infeasible. We have to consider the actual geometry of the master conductor.

For two separated polygons, we define their distance.

Definition 4: The aligned-box distance between two convex polygons A and B: $\text{dist}_a(A, B)$, is the edge length of the minimum axis-aligned square which touches both A and B.

Based on the aligned-box distance between a point and a polygon, we derive the following formula for calculating the aligned-box distance of two polygons [see Fig. 4(b)]:

$$\text{dist}_a(A, B) = \min\left\{\min_{1\le i\le n}\text{dist}_a(\boldsymbol{A}_i, B), \min_{1\le i\le m}\text{dist}_a(\boldsymbol{B}_i, A)\right\} \tag{5}$$

where $\boldsymbol{A}_i$ $(i = 1, 2, \ldots, n)$ is the vertices of polygon A and $\boldsymbol{B}_i$ $(i = 1, 2, \ldots, m)$ is the vertices of polygon B. It is obvious that for any two separated polygons A and B, $\text{dist}_a(A, B) > 0$.

The vertical distance between two conductor blocks is as follows.

Definition 5: The vertical distance between two 3-D conductor blocks A and B is

$$\text{dist}_v(A, B) = \max\{z_{\min}(A) - z_{\max}(B), z_{\min}(B) - z_{\max}(A)\}. \tag{6}$$

We set the horizontal distance between two conductor blocks as the aligned-box distance between their xoy-plane projections. Then, we have the 3-D distance between them.

Definition 6: The 3-D distance between two conductor blocks A and B is

$$\text{dist}(A, B) = \max\{\text{dist}_v(A, B), \text{dist}_a(P_A, P_B)\} \tag{7}$$

where P_A and P_B are the xoy-plane projections of A and B, respectively.

The idea for generating the Gaussian surface G_A for the master conductor A is to calculate the minimum distance $d_{\min}$ between A and its neighbor conductors and then make G_A about $d_{\min}/2$ distance away from A. It is guaranteed that such a Gaussian surface does not intersect any conductor. Based on the considered conductor geometry, the Gaussian surface surrounding the master conductor also forms a convex straight prism. In Fig. 4(b), the xoy projection of the Gaussian surface is shown. Each edge of master conductor A's projection is inflated outward to obtain an edge where every point's aligned-box distance to A is $d_{\min}/2$. Then, the edges obtained by inflation is connected by adding edges, resulting in the xoy projection of Gaussian surface G_A. If A's projection has n edges, the number of edges of G_A's projection is between n and $2n$. The Gaussian surface can be finally obtained after raising the xoy projection along the z-axis.

For the situation where the master conductor contains multiple blocks, the virtual Gaussian surface sampling technique [14] becomes useful. It allows us to construct and sample the Gaussian surface for each conductor block individually, without the necessity of calculating the envelope of the block Gaussian surfaces to get the whole Gaussian surface. For the non-Manhattan conductor block, the top or bottom face of its Gaussian surface is a general 2-D polygon. The sampling on this polygon can be carried out with the rejection sampling or other techniques [25].

C. Algorithm Using Manhattan Transition Cube

A natural idea is still using Manhattan (axis-aligned) transition cubes in the FRW algorithm for the structure with non-Manhattan conductors. During the random walk procedure, the 2-D aligned-box distance can be used to determine the Manhattan transition cube touching the side face of a non-Manhattan conductor. Suppose the current position of walk is $\boldsymbol{P}$ (x, y, z). What we want is the largest transition cube centered at $\boldsymbol{P}$ which does not intersect or contain any conductor. This is equivalent to calculating the minimum distance between point $\boldsymbol{P}$ and its nearby conductors. For a Manhattan conductor, calculating its distance to $\boldsymbol{P}$ is trivial. For a non-Manhattan conductor A, the distance is calculated as

$$\text{dist}_a(\boldsymbol{P}, A) = \max\{\text{dist}_v(\boldsymbol{P}, A), \text{dist}_a(\boldsymbol{P}, P_A)\} \tag{8}$$

where P_A stands for the *xoy* projection of A. The minimum of these distances is the half size of the Manhattan transition cube.

Because millions of hops are usually performed, the minimum distance between a point and its nearby conductors should be calculated as fast as possible. The space management technique has been proposed for this aim, which avoids traversing all conductors during the calculation. However, the existing technique only considers Manhattan conductors, and is not suitable for the problem involving non-Manhattan conductors. There are two strategies to settle this problem.

1) Employ Additional Structure for Non-Manhattan Objects: Assuming the majority of the conductors are of Manhattan shape, a simple approach is to first find the transition cube only taking Manhattan conductor blocks as obstacles and then shrink the cube by checking non-Manhattan conductor blocks one by one. The finally obtained transition cube does not cross any conductor, and is valid for performing an FRW hop. This approach only utilizes the space management technique for Manhattan structures [12], and can be easily implemented. It can be efficient only if there is very few non-Manhattan conductors.

Another approach is to construct an additional spatial structure for the non-Manhattan conductors, so that not all of them needs to be checked for obtaining the valid transition cube. To avoid the complex judgement of domination relationship regarding non-Manhattan objects, here we consider the simple grid structure without candidate list. The grid represents a 3-D uniform partition of the whole domain. For each grid cell, only the intersected non-Manhattan conductor blocks are recorded. During the random walk, after getting the transition cube restrained by Manhattan objects we only check the non-Manhattan blocks in the current cell and its neighbor region (e.g., its adjacent cells). Then, the transition cube is shrunk to become a conductor-free one. This treatment is similar to the approach with an incomplete candidate list [12]. With this approach, we avoid traversing all non-Manhattan objects for each FRW hop. However, since the domination relationship is not checked, this approach does not contribute to the optimal runtime and induces some memory overhead.

2) Modify the Space Management Technique to Accommodate Non-Manhattan Objects: A comprehensive solution is to extend the space management techniques to consider the non-Manhattan objects. The difficulty lies in judging the domination relationship of two conductor blocks. It cannot be implemented directly through Definition 1, because it is impossible to enumerate infinite points in cell T. For two Manhattan cuboids, the domination is actually judged by only inspecting a small point set within T.

Theorem 2: Suppose conductor blocks A, B and spatial cell T are all axis-aligned Manhattan shapes. The sufficient and necessary conditions of "A dominates B regarding T" are as follows.

1) $B \cap T = \emptyset$.
2) $(B^* \cap T) \subseteq (A^* \cap T)$, where A^* and B^* are the geometries got by inflating A and B by $\text{dist}(B, T)$, respectively. ■

To explain condition 2) in Theorem 2, we consider the points belonging to $B^* \cap T$. Because B^* is got by inflating B by $d = \text{dist}(B, T)$, $B^* \cap T$ is actually a portion of surfaces of B^* and T. Noting that the surface of B^* is the contour where every point has the constant distance d to B. So, for $\forall \boldsymbol{P} \in B^* \cap T$, $\text{dist}_a(\boldsymbol{P}, B) = d$. As A^* is got by inflating A by the same distance d, and $\boldsymbol{P} \in A^* \cap T$ due to the condition 2), $\text{dist}_a(\boldsymbol{P}, A) \leq d = \text{dist}_a(\boldsymbol{P}, B)$. Imaging A and B continue to inflate, which makes the distance contours with larger distance sweeping the rest of points in T. Because A's distance contour marches with the same speed as B's in all x, y, z directions, for a point $\boldsymbol{P}$ in T but not belonging to $B^* \cap T$, $\text{dist}_a(\boldsymbol{P}, A) \leq \text{dist}_a(\boldsymbol{P}, B)$ will still hold. This means A dominates B regarding T. Further, we can prove Theorem 2.

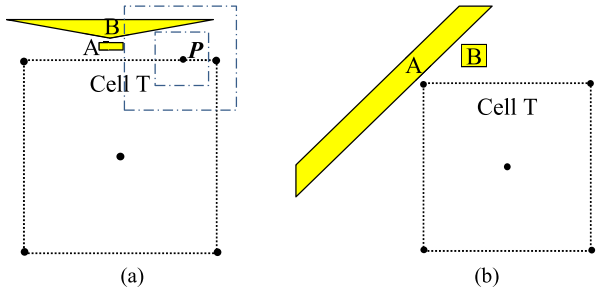

Fig. 5. Examples where A does not dominate B regarding T (a 2-D top view). (a) A is nearer to the points in $T \cap B^*$ than B, but $\boldsymbol{P}$ is closer to B. (b) A is nearer to the four vertices of T than B.

Based on Theorem 2, we can only consider the points in $B^* \cap T$ (which is a 2-D rectangle) for checking if A dominates B. This derives an efficient domination judgement algorithm for Manhattan objects [11], [12].

However, only inspecting the intersection of T and B^* is not sufficient for non-Manhattan objects. This is because the swept region during the march of a block's distance contour depends on the block's shape. For A and B with arbitrary shape, it is not guaranteed that A is nearer to the rest of points in T than B, providing A is nearer to the points in $B^* \cap T$ than B. In Fig. 5(a), we show such an example. Similarly, only inspecting the vertices of T is not sufficient either for judging the domination [see Fig. 5(b)].

Not like the situation for Manhattan conductors, there is not a feasible way for judging the domination of general non-Manhattan shapes. However, there are two obvious sufficient conditions for the domination relationship. Based on them we will develop a technique to judge the domination of non-Manhattan conductors.

Theorem 3: For two conductor blocks A and B, $\text{In}(A)$ denotes a Manhattan inscribed block of A, and $\text{Ex}(B)$ denotes a Manhattan external block of B.

1) If A dominates $\text{Ex}(B)$ regarding spatial cell T, A dominates B regarding T.
2) If $\text{In}(A)$ dominates B regarding spatial cell T, A dominates B regarding T. ■

A corollary of Theorem 3 is that, if $\text{In}(A)$ dominates $\text{Ex}(B)$, A dominates B. Therefore, with the domination check of two Manhattan blocks (using the approach based on Theorem 2) we can partially detect the domination relationship between two blocks in arbitrary shape. Fig. 6 shows examples involving non-Manhattan blocks, where the domination between A and B can be detected.

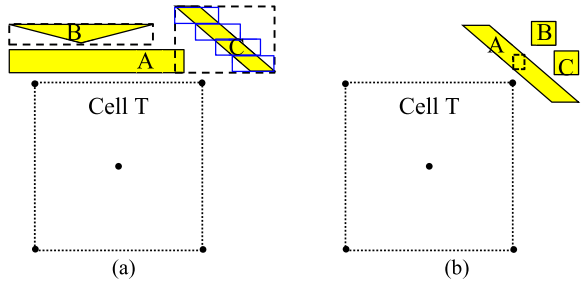

Fig. 6. With the Manhattan inscribed and external blocks and Theorem 3, we can partially detect the domination relationship of non-Manhattan shapes. (a) A dominates B because A dominates Ex(B). (b) A dominates B because In(A) dominates B. It is not easy to detect the domination of A to C.

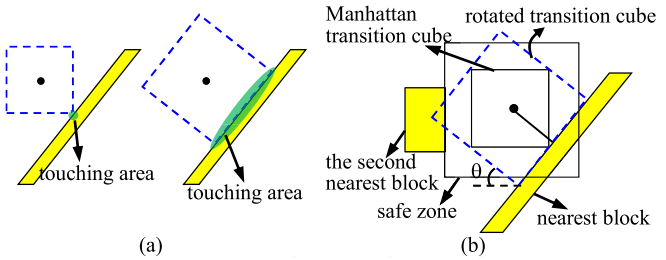

Fig. 7. Top view of non-Manhattan conductors and transition cubes. (a) Manhattan transition cube versus rotated transition cube. (b) Rotated transition cube can be accepted only if it is within the safe zone.

It should be pointed out, for some non-Manhattan shape (e.g., long bevel wire) its Manhattan inscribed block and external block are much different from itself. Therefore, the approach based on Theorem 3 often fails to detect the domination relationship. For example, in Fig. 6 it fails to detect that A dominates C. To improve this situation, we propose Theorem 4.

Theorem 4: For two conductor blocks A and B, a set of Manhattan blocks $\{B_i\}$ fullfils $\cup B_i \supseteq B$, and a set of Manhattan blocks $\{A_i\}$ fullfils $\cup A_i \subseteq A$.

1) If for any i, A dominates B_i regarding spatial cell T, A dominates B regarding T.
2) If $\cup A_i$ dominates B regarding spatial cell T, A dominates B regarding T. ■

Theorem 4 is an extended version of Theorem 3, and can be easily proved. The condition 1) in Theorem 4 can be easily judged if A is a Manhattan block. For a Manhattan block B, the condition 2) in Theorem 4 can also been judged based on Theorem 2, though handling $\cup A_i$ is more complex than handling a single Manhattan cuboid.

With Theorem 4 we can improve the algorithm judging the domination of non-Manhattan conductors. The idea is representing a non-Manhattan block with a set of Manhattan blocks, and then judging the domination of Manhattan block set with Theorem 4. In Fig. 6(a), with C represented by four Manhattan blocks (outlined in blue) the algorithm is able to detect that A dominates C. The choice of the set of Manhattan blocks affects both success rate of domination check and computing time. While judging the domination between two non-Manhattan blocks, the time cost increases a lot if both blocks are represented by many Manhattan blocks. This usually overwhelms the benefit got from correctly detecting the domination relationship. So, we should restrict the size of the Manhattan block set for representing a non-Manhattan block.

In the algorithm checking if a conductor should be added to a candidate list (Algorithm 1), the distance between the spatial cell and conductor B "$d(B, T)$" is calculated. This distance has the same meaning as that in Definition 6. To reduce the computing cost, we consider the cell T with 3-D cube shape, which exists in the grid or grid-octree hybrid spatial structures [12]. Then

$$\text{dist}(B, T) = \text{dist}_a(\boldsymbol{P}, B) - l/2 \tag{9}$$

where l is the size of cell T, and $\boldsymbol{P}$ is the center point of T. With (9), the distance between the spatial cell and conductor B can be calculated quickly. Now, Algorithm 1 can be executed with input of a non-Manhattan conductor, and the space management structure with candidate list can be generated.

Because the sufficient conditions are used to judge the domination relationship of non-Manhattan conductor blocks, the proposed method might fail to detect the domination relationship, especially for long bevel wires. This weakens the benefit of the space management technique. To overcome this drawback, we perform a preprocess step to cut each long bevel wire into short segments. This increases the total number of conductor blocks for simulation, but may improve the effectiveness of the space management involving non-Manhattan conductors. In practice, we uniformly cut the bevel wire into segments such that the longest edge of each segment is at most 5× longer than its shortest edge.

D. Algorithm Using Rotated Transition Cube

Instead of always using Manhattan transition cubes in the FRW algorithm, another idea is using rotated transition cube if possible. The latter's potential benefit is larger transition cube and touching area, as illustrated in Fig. 7(a). This idea has been adopted for extracting the capacitances of cylindrical TSV structures, and brings about 2× speedup [19]. To apply it to our problem, we first give a definition.

Definition 7: The 2-D *rotated-box distance* between a 2-D point $\boldsymbol{P}$ (x, y) and a convex polygon A with vertices $\boldsymbol{A}_1$, $\boldsymbol{A}_2, \ldots, \boldsymbol{A}_n$ in anti-clockwise order is

$$\text{dist}_r(\boldsymbol{P}, A) = \max\left\{\max_{1\le i\le n} \frac{(x - x_i)(y_{i+1} - y_i) - (y - y_i)(x_{i+1} - x_i)}{\sqrt{(x_{i+1} - x_i)^2 + (y_{i+1} - y_i)^2}}, \text{dist}_a(\boldsymbol{P}, B_A)\right\} \tag{10}$$

where B_A is the Manhattan bounding box of A, and (x_i, y_i) is the coordinates of $\boldsymbol{A}_i$.

The rotation of transition cube is in the *xoy* plane. So, the 2-D rotated-box distance (Definition 7) is useful. It corresponds to either a transition square adjoining polygon A's edge, or a Manhattan square touching A's vertex. As shown in Fig. 8(a), this rotated transition cube well fits conductor A's side face, or is a larger Manhattan cube (like for point $\boldsymbol{P}_3$). Similar to the calculation of $\text{dist}_a(\boldsymbol{P}, A)$, for $\text{dist}_r(\boldsymbol{P}, A)$ the maximum of the perpendicular distances to A's visible edges

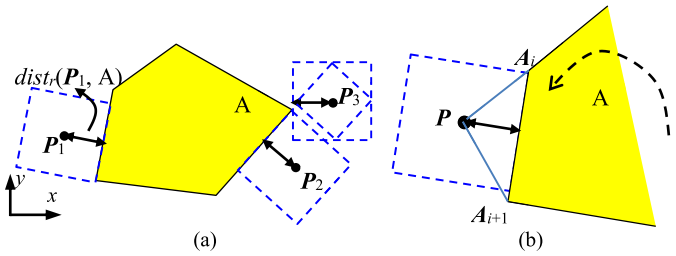

Fig. 8. Illustration of the 2-D rotated-box distance between a point and a polygon. (a) Rotated-box distances between A and three nearby points. (b) Illustration for the calculation of $\text{dist}_r(\boldsymbol{P}, A)$.

is pursued. The formula for this perpendicular distance is explained in Fig. 8(b). Comparing (3) and (10), we see that $\text{dist}_r(\boldsymbol{P}, A) \geq \text{dist}_a(\boldsymbol{P}, A)$.

During the FRW procedure, we inquiry the nearest conductor for current position $\boldsymbol{P}$ in terms of the aligned-box distance. If the obtained conductor, say A, is a non-Manhattan block, we can rotate the transition cube trying to get a larger transition cube. The rotated-box distance between $\boldsymbol{P}$ and A is calculated

$$\text{dist}_r(\boldsymbol{P}, A) = \max\{\text{dist}_v(\boldsymbol{P}, A), \text{dist}_r(\boldsymbol{P}, P_A)\} \tag{11}$$

where P_A stands for the *xoy*-plane projection of A. If it is larger than $\text{dist}_a(\boldsymbol{P}, A)$, the corresponding rotated transition cube is certainly not a Manhattan one and adjoins A's side face.

A prerequisite for using the rotated transition cube is that it does not intersect any other conductor [see Fig. 7(b)]. We must examine that, as has been done in [19]. We can take the Manhattan transition cube touching the second nearest conductor block as a safe zone. The rotated transition cube is accepted only if it is within the safe zone. Otherwise, we have to use the smaller Manhattan transition cube for this FRW hop. So, the remaining question is how to calculate the size of this safe zone.

If there is no non-Manhattan space management used, i.e., we traverse the non-Manhattan blocks to find the nearest conductor, the second nearest block is known. With it we get the safe zone. If the approach with an additional grid structure for non-Manhattan conductors is employed, the second nearest block is also available.

It should be pointed out, that the same problem occurs in [19]. The solution therein is to additionally treat each TSV's neighbor region as a spatial cell and generate the candidate list for it. Because there are relatively fewer TSVs, and other conductors are all regarded as Manhattan cuboids facilitating the generation of candidate list, that approach demonstrates good efficiency. However, the problem considered in this paper may include a large number of non-Manhattan blocks, and the domination judgement for generating the candidate list is much more complicated. The approach in [19] could not be efficient for the considered non-Manhattan conductor structures.

If the space management employs the candidate list and treats all conductors as a whole, like the approach proposed in the last section, only the nearest conductor can be obtained by inquiring the candidate list. How to efficiently obtain the second nearest conductor and further the safe zone becomes a problem. To solve it, we propose to modify the domination check to reduce the difficulty of finding the second nearest conductor. We define a strong domination relationship for non-Manhattan conductor block, with which finding the second nearest conductor becomes unnecessary.

Algorithm 2 CandidateCheck2 (Conductor Block B, Cell T)

```
d := dist_a(B, T); l is the size of T;
If d ≥ L(T) then return false;
For each b in the candidate list of T do
    If b is non-Manhattan and b strongly dominates B or b
      is Manhattan and b dominates B, then return false;
    Elseif B is non-Manhattan and B strongly dominates b
      or B is Manhattan and B dominates b then
        Remove b from the candidate list of T;
    Endif
Endfor
Add B to the candidate list of T;
If (d + l) < L(T) then L(T) := d + l;
return true.
```

Definition 8: T is a spatial cell, and B_1, B_2 are two conductor blocks, where B_1 is a non-Manhattan block. If for any point $\boldsymbol{P} \in T$, and $\boldsymbol{P} \notin B_1 \cup B_2$, $\text{dist}_a(\boldsymbol{P}, B_1) \leq 0.5 \times \text{dist}_a(\boldsymbol{P}, B_2)$, we say B_1 *strongly dominates* B_2 regarding T.

Theorem 5: Suppose a non-Manhattan conductor block A is the nearest conductor to point $\boldsymbol{P}$ in terms of aligned-box distance, and B is the second nearest conductor. If $\text{dist}_a(\boldsymbol{P}, A) \leq 0.5 \times \text{dist}_a(\boldsymbol{P}, B)$, the rotated transition cube for $\boldsymbol{P}$ must not intersect B and any other conductor. ■

Proof: According to the definitions of the 2-D aligned-box distance and rotated-box distance, we see that $\text{dist}_r(\boldsymbol{P}, A) \leq \sqrt{2}\text{dist}_a(\boldsymbol{P}, A)$. This is also evident if we comparing (3) and (10). Then, if $\text{dist}_a(\boldsymbol{P}, A) \leq 0.5 \times \text{dist}_a(\boldsymbol{P}, B)$

$$\text{dist}_a(\boldsymbol{P}, B) \geq 2\text{dist}_a(\boldsymbol{P}, A) \geq \sqrt{2}\text{dist}_r(\boldsymbol{P}, A). \tag{12}$$

As shown in Fig. 7(b), the rotated transition cube for $\boldsymbol{P}$ is within an axis-aligned cube whose half size is $(\sin\theta+\cos\theta)\text{dist}_r(\boldsymbol{P}, A)$. This half size is not larger than $\sqrt{2}\text{dist}_r(\boldsymbol{P}, A)$. It is therefore no larger than $\text{dist}_a(\boldsymbol{P}, B)$, due to (12). So, the rotated transition cube is within the safe zone restrained by B. This proves Theorem 5.

Below, we give a corollary of Theorem 5.

Theorem 6: Suppose a non-Manhattan conductor block A is the nearest conductor to point $\boldsymbol{P}$ in terms of aligned-box distance. If A strongly dominates another conductor block B regarding to a spatial cell containing $\boldsymbol{P}$, the rotated transition cube for $\boldsymbol{P}$ must not intersect B. ■

Based on Theorem 6, we can modify the procedure checking if conductor block B should be added to the candidate list of T, as described in Algorithm 2.

Now, when we inquire the space management structure and find a non-Manhattan conductor block as the nearest conductor, we need not worry about finding the second nearest conductor for checking the validity of the rotated transition cube. If the second nearest conductor is not in the candidate list, it must be strongly dominated by the nearest non-Manhattan block, so that the rotated transition cube is within the safe zone. Otherwise, by inquiring the candidate

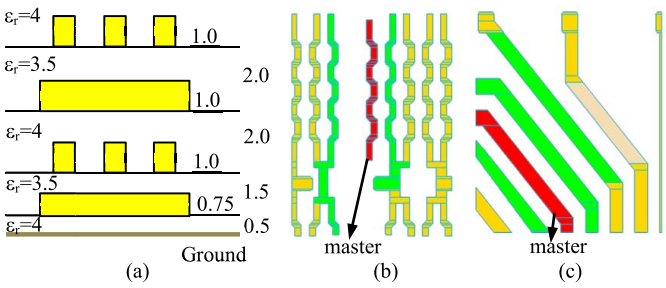

Fig. 9. Geometry information of test cases 1–4. (a) Cross section of the process technology. The thickness of each dielectric layer and the height of metal are labeled (in unit of μm). (b) and (c) Top view of two examples of metal layers.

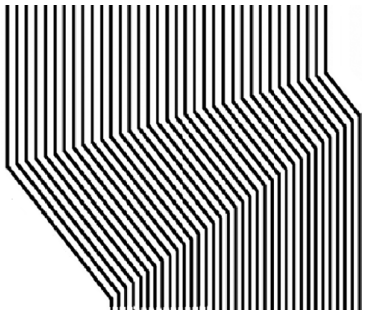

Fig. 10. Top view of the package interconnect structure composed of m-lossy conductors (cases 5–7) [8].

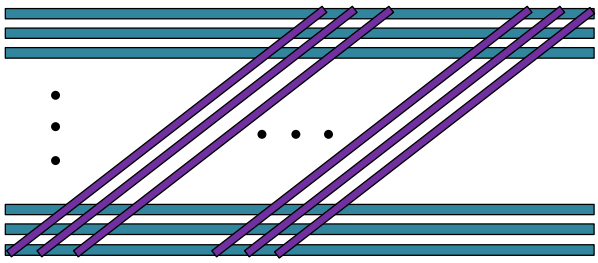

Fig. 11. Top view of a structure with two metal layers (case 8).

list we can find the second nearest conductor and get the safe zone. Therefore, by modifying the construction of space management with the strong domination relationship, we can easily examine the prerequisite for using the rotated transition cube.

It should be pointed out that Definition 8 itself does not result in a judgement algorithm. In practice, the strong domination is judged based on the domination check technique for non-Manhattan conductor, which utilizes the sufficient conditions in Theorems 3 and 4. The condition of strong domination is much stricter than that of domination. As compared with the method using Manhattan transition cube, more conductors cannot be excluded from inserting into the candidate list. This brings some negative effect to the efficiency of the space management technique.

IV. Numerical Results

Based on the C++ program RWCap [11], [13], we have implemented the proposed FRW algorithms for extracting the capacitances of non-Manhattan conductor structures. The grid-octree hybrid space management structure and the fast candidate list generation techniques in [12] are employed, as the basis of the proposed techniques for handling non-Manhattan conductors. The termination criterion for all FRW-based algorithms is set to 0.5% 1-σ error.

All experiments are carried out on a Linux server with Intel Xeon E5-2650 2.0 GHz CPU. All results are obtained from execution of serial computing.

A. Test Cases

The test cases are described as follows.

Cases 1–4: Got from layout of a mixed-signal circuit design (see Fig. 9). The minimum wire width in each case is about 0.4 μm. For each case, there is from 90 to 516 conductor blocks in four metal layers. From bottom to top, the dielectric layers have relative permittivity of 4.0 and 3.5 alternatively. In Fig. 9(b) and (c), we show two examples of the metal layer's layout (the master conductor is in red), where there are some non-Manhattan conductor blocks.

Cases 5–7: A package interconnect composed of m lossy conductors embedded in a uniform dielectric [8], as shown in Fig. 10. The m is chosen as 8, 16, and 32, respectively. The width and height of each wire are 0.12 and 0.2 μm, respectively. For each case, the conductor in the middle is set as the master conductor.

Case 8: A structure with two metal layers, as shown in Fig. 11. The first layer includes 50 aligned wires parallel to the x-axis, and the second layer includes 50 40°-angled bevel wires. The distance between two layers of wires is 0.36 μm. The width and height of each wire are 0.12 and 0.2 μm, respectively. The length of wire is about 35 μm.

Cases 9–12: Formed by duplicating cases 1–4 for 2×2 times. The number of conductors in these larger cases ranges from 360 to 2064.

We first test the algorithms using Manhattan transition cube, which employ the techniques in Section III-C. The results are compared with a fast capacitance solver based on BEM, QBEM [5]. Then, the techniques with the rotated Manhattan transition cube in Section III-D are tested. After that, more experiments are carried out to further validate the accuracy, efficiency and versatility of the proposed techniques.

The tested algorithms are as follows.

Alg. 1: The FRW algorithm based on Manhattan transition cubes, with the approach traversing non-Manhattan conductors.

Alg. 2: The FRW algorithm based on Manhattan transition cubes, with an additional grid spatial structure for non-Manhattan conductors.

Alg. 3: The FRW algorithm based on Manhattan transition cubes, with the modified space management technique.

Alg. 4: The FRW algorithm using rotated transition cube, with the approach traversing non-Manhattan conductors.

Alg. 5: The FRW algorithm using rotated transition cube, with an additional grid spatial structure for non-Manhattan conductors.

TABLE I
COMPARISON OF A FAST BEM SOLVER AND THE PROPOSED FRW METHODS USING MANHATTAN TRANSITION CUBE

Case	#conductor	#non-Manhattan conductor	QBEM				FRW			FRW's CPU time (s)			SP_{Alg1}^{Alg2}	SP_{Alg1}^{Alg3}	SP_{QBEM}^{Alg3}
			#panel	Mem.	Cap.(aF)	Time(s)	#walk	Mem.	Cap.(aF)	Alg. 1	Alg. 2	Alg. 3			
1	90	28	20377	101MB	173.3	2.88	260K	<1MB	176.1	5.02	2.07	1.76	2.4	**2.9**	**1.6**
2	264	134	64062	982MB	264.9	28.6	295K	<1MB	266.4	21.1	3.12	2.56	6.8	**8.2**	**11**
3	378	188	68001	1.4GB	406.1	51.3	394K	<1MB	413.4	35.8	5.85	4.73	6.1	**7.6**	**11**
4	516	310	83923	1.6GB	489.5	55.5	208K	1.1MB	486.9	24.2	1.95	1.56	12	**16**	**36**
5	24	8	9170	103MB	585.0	3.24	361K	<1MB	600.1	10.63	6.15	4.31	1.7	**2.5**	**0.8**
6	48	16	11920	180MB	586.7	5.74	355K	1.1MB	595.6	16.17	7.23	3.86	2.2	**4.2**	**1.5**
7	96	32	15980	324MB	584.8	10.3	321K	1.5MB	599.0	26.2	6.07	3.48	4.3	**7.5**	**3.0**
8	100	50	38158	550MB	1218	42.4	370K	2.6MB	1275	27.7	23.0	5.82	1.2	**4.8**	**7.3**
9	360	112	--	--	--	--	260K	<1MB	176.4	16.81	2.19	1.60	7.7	**11**	--
10	1056	536	--	--	--	--	291K	1.7MB	268.3	111.7	3.40	2.70	33	**41**	--
11	1512	752	--	--	--	--	393K	2.5MB	412.6	167.2	6.61	4.77	25	**35**	--
12	2064	1240	--	--	--	--	206K	3.7MB	480.3	132.1	2.11	1.58	62	**84**	--

SP_{Alg1}^{Alg2} is the speedup of Alg. 2 over Alg. 1. SP_{Alg1}^{Alg3} is the speedup of Alg. 3 over Alg. 1. SP_{QBEM}^{Alg3} is the speedup of Alg.3 over QBEM.

Alg. 6: The FRW algorithm using rotated transition cube, with the modified space management technique.

In Sections IV-B–IV-D, the dielectrics in all test cases are changed to get a uniform dielectric with relative permittivity of 1. In Section IV-E, the multi-dielectric structures, i.e., cases 1–4 and 9–12, are extracted.

B. Results of Algorithms Using Manhattan Transition Cube

The 12 test cases are extracted with Algs. 1–3 and QBEM, whose results are compared in Table I. "Cap." is the self-capacitance of the master conductor, while "Mem." stands for the memory usage. Because Algs. 1–3 produce almost same capacitance results (with less than 2% stochastic discrepancy), we only list the capacitance results got from Alg. 3. QBEM employs an automatic boundary discretization and is able to extract the capacitances accurately. From Table I, we see that the discrepancy of QBEM and the FRW algorithms in the capacitance result is fairly small, i.e., within 2.5%. Note that the Neumann boundary is assumed for the extraction with QBEM [5], such that the self-capacitance got with the FRW algorithm is always larger than that got with QBEM. The results validate the correctness of the proposed techniques for extracting the non-Manhattan conductor structures.

In Table I, the different performance of Algs. 1–3 is also demonstrated. Utilizing the space management (Algs. 2 and 3) makes the CPU time dramatically reduced, as compared with Alg. 1. The speedup ratio increases with the number of non-Manhattan conductors in the test case, and is up to 84× for the largest case. While comparing Algs. 2 and 3, we see that the latter is usually 1.2×–1.9× faster than the former. For case 8, Alg. 3 becomes even 4× faster than Alg. 2, as it performs each hop much faster due to shorter candidate lists. More details of the three algorithms are listed in Table II. From the table, we see that the average number of hops per walk (#hop) is almost the same for Algs. 1 and 3. #hop increases a little bit in Alg. 2, due to the setting of neighbor region and the incomplete candidate list technique used. Within Alg. 3, the candidate lists considering the domination of non-Manhattan conductors are generated. Therefore, Alg. 3 consumes more time (T_{sp}) for constructing space management structure but costs much less memory for the spatial data structure (Mem_{sp}), as compared with Alg. 2. It should be pointed out that the strategies used in Alg. 1 ∼ 3 do not affect the number of walks (#walk). So, it is not listed in Table II.

For the comparison of the FRW-based algorithms and QBEM, let us look at Table I again. We can see that Alg. 3 is up to 36× faster than QBEM for the first eight cases. For the last four larger cases, QBEM's result is not available due to the excessive demand of memory usage. The speedup ratio roughly increases with the size of test case. As for the memory usage, the FRW-based algorithm shows huge advantage. These results reflect the major difference between the BEM and FRW method for capacitance extraction problem.

C. Results of Algorithms Using Rotated Transition Cube

Based on the strategy that allows the transition cube to rotate, we have developed Algs. 4–6. Their computational results are listed in Table II as well, for better comparison among Algs. 1–6. We have verified that their capacitance results are all correct, which are not included in Table II. Alg. 4 uses the approach based on traversing the non-Manhattan conductors. Comparing Alg. 4 with Alg. 1, we see that the idea of rotating the transition cube could bring 1.47× on average and up to 2.1× speedup. This is mainly caused by the reduction of the number of hops per walk (#hop). While comparing the data of Algs. 3 and 6, we can see that utilizing the rotated transition cube is still advantageous, but with a reduced speedup ratio (∼1.2× on average and up to 1.6×). This is due to the negative effect of using the strong domination check in space management. Similar to the algorithms using Manhattan transition cube, the modified space management handling all conductors as a whole (Alg. 6) excels the approach using an additional grid structure (Alg. 5), in terms of overall runtime and the memory cost. The benefit is similar to that of Algs. 3 to Alg. 2.

If comparing Alg. 6 with Alg. 1, we see that the speedup ratio ranges from 2.9× to 96×. It is contributed by the idea of rotating transition cube, and the sophisticated techniques for domination check and candidate list generation during the

TABLE II
DETAILED COMPARISON OF DIFFERENT FRW METHODS USING MANHATTAN TRANSITION CUBE AND THE RESULTS OF THE PROPOSED FRW METHODS USING ROTATED TRANSITION CUBE

Case	Alg. 1		Alg. 2				Alg. 3				Alg. 4			Alg. 5			Alg. 6			
	#hop	Time(s)	#hop	T_{sp} (s)	Mem_{sp}	Time(s)	#hop	T_{sp} (s)	Mem_{sp}	Time(s)	#hop	Time(s)	SP_{Alg1}^{Alg4}	#hop	Mem_{sp}	Time(s)	#hop	Mem_{sp}	Time(s)	SP_{Alg1}^{Alg6}
1	15	5.02	17	0	2.1MB	2.07	15	0	<0.1MB	1.76	13.5	4.68	1.1	15.5	2.1MB	1.92	13.5	<1MB	1.73	**2.9**
2	16.9	21.1	17.9	0	2.5MB	3.12	16.8	0	0.1MB	2.56	13.2	16.48	1.3	14.1	2.5MB	2.79	13.2	<1MB	2.43	**8.7**
3	30.2	35.8	33.3	0.01	3.1MB	5.85	30.3	0.01	0.1MB	4.73	14.2	18.60	1.9	17.3	3.1MB	3.66	14.2	<1MB	2.95	**12**
4	13.3	24.2	13.3	0.01	2.5MB	1.95	13.3	0.02	0.1MB	1.56	10.7	18.10	1.3	10.7	2.5MB	1.76	10.7	<1MB	1.41	**17**
5	24.8	10.63	27.6	0	1.8MB	6.15	25.5	0.01	0.1MB	4.31	14.8	7.20	1.5	17.6	1.8MB	4.11	15.1	<1MB	5.13	**2.1**
6	23.7	16.17	25.8	0	2MB	7.23	24.4	0.02	0.3MB	3.86	14.3	11.47	1.4	16.3	2.1MB	4.64	14.7	2.3MB	3.35	**4.8**
7	22.1	26.2	23.7	0	2.5MB	6.07	22.8	0.03	0.4MB	3.48	13.8	18.57	1.4	15.4	2.5MB	4.06	16.2	<1MB	3.61	**7.3**
8	30.7	27.7	30.8	0.01	2.1MB	23.0	34.2	0.14	0.9MB	5.82	13.4	12.99	2.1	13.6	2.1MB	10.43	17.0	<1MB	3.81	**7.3**
9	14.5	16.81	15.2	0	2MB	2.19	14.5	0.01	<0.1MB	1.60	12.9	14.77	1.1	13.6	2MB	1.97	12.9	<1MB	1.58	**11**
10	16.5	111.7	17.1	0.02	2.6MB	3.40	16.5	0.03	0.3MB	2.70	12.8	86.64	1.3	13.4	2.6MB	2.99	12.8	<1MB	2.41	**46**
11	30	167.2	31.5	0.03	3.5MB	6.61	30.2	0.05	0.4MB	4.77	13.9	88.53	1.9	15.5	3.5MB	3.87	14.2	1MB	3.04	**55**
12	13.3	132.1	13.3	0.03	2.9MB	2.11	13.3	0.07	0.9MB	1.58	10.7	99.10	1.3	10.7	2.9MB	1.87	10.9	2.1MB	1.37	**96**

SP_{Alg1}^{Alg4} is the speedup of Alg. 4 over Alg. 1. SP_{Alg1}^{Alg6} is the speedup of Alg. 6 over Alg. 1.

TABLE III
COMPUTATIONAL RESULTS FOR TWO CROSSOVERS AND THEIR TILTED COUNTERPARTS (CAPACITANCE IN UNIT OF aF, TIME IN UNIT OF SECOND)

Structure	RWCap2				Alg. 1		Alg. 3		Alg. 6			
	#walk	#hop	Time	Cap.	Time	Cap.	Time	Cap.	Time	Cap.	#walk	#hop
50x50	248K	11.3	1.17	856	76.7	853	10.3	853	6.7	855	488K	22.9
100x100	152K	8.4	0.54	120	40.0	120	6.7	120	5.2	120	418K	11.6

TABLE IV
COMPUTATIONAL RESULTS FOR A STRUCTURE WITH ONLY 5.5% NON-MANHATTAN CONDUCTOR BLOCKS (CAPACITANCE IN UNIT OF aF, TIME IN UNIT OF SECOND)

Case	QBEM		Alg.1	Alg.2	Alg.3	Alg.4	Alg.5	Alg.6		SP_{Alg1}^{Alg3}	SP_{QBEM}^{Alg3}
	Cap.	Time	Time	Time	Time	Time	Time	Cap.	Time		
1	173.3	2.88	5.02	2.07	1.76	4.68	1.92	176.1	1.73	**2.9**	**1.6**
1a	176	2.82	3.45	1.65	1.26	3.38	1.57	180	1.31	**2.7**	**2.2**

SP_{Alg1}^{Alg3} is the speedup of Alg. 3 over Alg. 1. SP_{QBEM}^{Alg3} is the speedup of Alg. 3 over QBEM.

space management. The latter essentially would bring larger acceleration for structures involving a lot of non-Manhattan conductors. As compared with QBEM's results in Table I, we see that Alg. 6 has at most 39× speedup for case 4.

D. Further Accuracy and Efficiency Validation

Two crossover structures are tested to further validate the accuracy of the proposed algorithms. The first one is derived from case 8. The only difference between it and case 8 is that the wires in the second layer are perpendicular to those in the first layer. This produces a 50 × 50 crossover case. The other one is the 100 × 100 crossover case in [12]. Since the both crossover structures are of Manhattan structure, they can be simulated with the existing FRW solvers, like RWCap2 [12], [13]. We rotate each of them with a 40° angle to obtain its non-Manhattan counterpart, and then simulate it with the proposed algorithms. The results are listed in Table III. From the table, we see that the capacitance results of the tilted structures well match those of the original cases. This validates the accuracy of the proposed techniques. Note that the result for the 100×100 crossover also matches that in [12]. Because more FRW walks, hops per walk and operations for performing a hop are needed for handling a non-Manhattan structure, the proposed algorithms are several times slower than the FRW algorithm which only deals with Manhattan geometries. While comparing Algs. 1 and 6, we see that the proposed techniques bring 11× and 8× speedup respectively, for the two crossover structures.

In order to see how the proposed techniques perform for a structure with fewer non-Manhattan geometries, we modify case 1 to "case 1a" which includes only five non-Manhattan blocks among the total 90 conductor blocks. The computational results are listed in Table IV, along with those for case 1 for comparison.

From Table IV, we see that the acceleration brought by the proposed techniques changes little for the case with fewer non-Manhattan conductors. Meanwhile, because the fewer non-Manhattan conductors result in faster computation of the FRW-based method, the speedup over QBEM increases from 1.6× to 2.2×. We also modify case 1a to obtain a structure with zero non-Manhattan conductor (case 1b). It can be simulated with RWCap2 with a runtime of 1.23 s. This is only slightly less than that of the proposed method for case 1a (1.26 s). It suggests that, although the proposed method has to scarify some runtime for the ability of handling non-Manhattan geometry, the runtime overhead is almost proportional to the ratio of non-Manhattan conductor in the simulated structure. For a structure including very few non-Manhattan conductors, like case 1a, the increase of runtime compared with the conventional FRW method simulating a similar Manhattan structure can be very little. Note that, in the preceding experiment with crossover structures, the simulated tiled structure includes 100% non-Manhattan conductors, and therefore makes the proposed FRW method much slower than the conventional FRW method.

Because the whole capacitance matrix is sometimes needed, we add the following experiment. For case 7, which is a package structure including 32 wires, we extract the whole

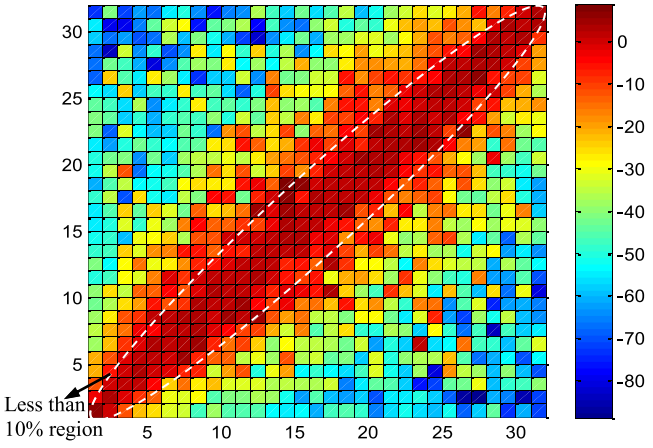

Fig. 12. Capacitance discrepancy (in percentage) between Alg. 6 and QBEM for the whole capacitance matrix.

TABLE V
RUNTIMES OF THE PROPOSED ALGORITHMS AND QBEM FOR EXTRACTING THE WHOLE CAPACITANCE MATRIX (TIME IN UNIT OF SECOND)

Case	QBEM	Alg.1	Alg.2	Alg.3	Alg.4	Alg.5	Alg.6	SP_{Alg1}^{Alg6}	SP_{QBEM}^{Alg6}
7	313.6	959.1	194.1	135.8	667.4	129.4	97.3	**9.9**	**3.2**

SP_{Alg1}^{Alg6} is the speedup of Alg. 6 over Alg. 1. SP_{QBEM}^{Alg6} is the speedup of Alg. 6 over QBEM.

capacitance matrix with our algorithms and QBEM. The runtimes are listed in Table V. And, the relative discrepancies of capacitance items obtained with the both methods are shown in Fig. 12. The QBEM's result is regarded as the standard.

The results show that, with Alg. 6 we only need 1.5 min to extract the whole 32×32 capacitance matrix. It means an average runtime of 3.04 s for the extraction with a single master conductor. As for QBEM, it costs 313.6 s, which is 3.2× more than Alg. 6. The speedup (9.9×) achieved with the proposed techniques is similar to the situation where there is only one master (see Tables I and II). Because the termination criterion of FRW-based algorithms is set regarding the self-capacitance, we cannot expect the coupling capacitances (the off-diagonal matrix entries) has the same accuracy as the self-capacitance. Take conductor no. 16 in case 7 as an example. Its self-capacitance is about 590 aF, while only its neighbor conductors (nos. 12–15 and 17–20) have coupling capacitance larger than 5.9 aF, i.e., 1% of the self-capacitance. So, much fewer random walks terminate on the non-neighbor conductors, which results in large stochastic error on the corresponding trivial coupling capacitances. This then causes the large discrepancy or error on the off-diagonal matrix entries shown in Fig. 12. In this experiment, we see that for the major coupling capacitances (between conductors not far from each other) the proposed FRW method has satisfied accuracy (less than 10% discrepancy to QBEM's result). If for some reason we shall pursue more accuracy of coupling capacitance, we can modify the termination criterion of FRW algorithm, or equivalently run more random walks.

It should be pointed out, that the deterministic method may exhibit performance advantage while extracting the capacitance matrix. It happens when the advanced direct equation solver [26], instead of iterative equation solver as in QBEM, is employed. Not only the generation of coefficient matrix but also the matrix factorization, which is the most time consuming part, needs to be executed only once. Therefore, the large runtime benefit can be attained. On the contrary, there is less benefit for the FRW-based method to make the capacitance-matrix extraction. Only the space management structure can be built once for a structure. It saves some total runtime of the FRW-based method.

E. Results of Multi-Dielectric Cases

For the multi-dielectric cases, we have built the surface Green's function and weight value tables with the TechGFT program [11], which are needed by the FRW algorithms. The results of QBEM and our methods are listed in Table VI. For the larger cases, the results of QBEM are not available. From the table, we can see that self-capacitances obtained by both methods have less than 2.5% discrepancy. And, the speedup of the proposed algorithm (Alg. 6) to QBEM is up to 29×. While comparing the different versions of the FRW method, we see that Alg. 6 has up to 91× speedup over Alg. 1, which is similar to the situation of single-dielectric cases. The results demonstrate that the proposed techniques are also suitable for the extraction of multi-dielectric structures.

F. Summary and Discussion

We first summarize the numerical results with the following remarks.

Remark 1: The proposed FRW techniques are able to accurately handle the general non-Manhattan conductor structure. Their capacitance results are validated for accuracy, and well correlate with those of QBEM [5].

Remark 2: Compared with the approach traversing non-Manhattan conductors for constructing the transition cubes, the proposed space management technique with domination judgement is 2.9×–84× faster. The largest speedup is achieved for a test case with 1240 non-Manhattan conductor blocks.

Remark 3: The strategy of using rotated transition cubes could bring at most 2.1× speedup, compared with the approach only using Manhattan transition cubes. Along with proposed space management technique based on the domination judgement of non-Manhattan conductor, the proposed algorithm is up to 96× faster than the simply extended FRW algorithm.

Remark 4: Compared with the approach using an additional grid spatial structure, the modified space management technique with candidate list brings up to 4× speedup to the FRW procedure, while consuming much less memory.

Remark 5: For the test cases, the proposed FRW algorithm is up to 39× faster than QBEM, with several orders of magnitude less memory usage.

Remark 6: Although the proposed method has to scarify some runtime for the ability of handling non-Manhattan geometry, its runtime overhead is about proportional to the ratio of

TABLE VI
COMPARISON OF A FAST BEM SOLVER AND THE PROPOSED FRW METHODS FOR MULTI-DIELECTRIC CASES

Case	#conductor	#non-Manhattan conductor	QBEM				FRW				FRW's CPU time (s)			SP_{Alg1}^{Alg6}	SP_{QBEM}^{Alg6}
			#panel	Mem.	Cap.(aF)	Time(s)	#walk	#hop	Mem.	Cap.(aF)	Alg. 1	Alg. 3	Alg. 6		
1	90	28	20377	100MB	667.8	2.89	300K	16.5	11.3MB	682.5	7.39	2.65	2.61	2.8	**1.1**
2	264	134	64062	985MB	1023	28.5	886K	15.6	11.6MB	1040	76.5	9.51	8.87	8.6	**3.2**
3	378	188	68001	1.42GB	1573	51.2	423K	15.8	11.6MB	1602	42.2	5.64	3.75	11	**14**
4	516	310	83923	1.65GB	1801	55.8	240K	12.1	12.1MB	1781	29.2	2.09	1.92	15	**29**
9	360	112	--	--	--	--	304K	16.4	11.5MB	680.8	25.5	2.52	2.41	11	--
10	1056	536	--	--	--	--	865K	15.4	12.8MB	1038	382.5	9.57	9.29	41	--
11	1512	752	--	--	--	--	424K	16.1	13.4MB	1600	200.8	5.96	3.88	52	--
12	2064	1240	--	--	--	--	238K	12.1	15.0MB	1785	172.4	2.01	1.89	91	--

SP_{Alg1}^{Alg6} is the speedup of Alg. 6 over Alg. 1. SP_{QBEM}^{Alg6} is the speedup of Alg.6 over QBEM.

non-Manhattan conductor blocks in the simulated structure. This means we scarify little runtime overhead for the structure with few non-Manhattan conductors.

From the results we see that the strategy of rotating the transition cube does not bring large speedup. It actually can be slightly slower than the algorithm only using Manhattan transition cube, if the simulated structure includes very few non-Manhattan conductors. This seems not consistent with the remarkable increase of touching area as shown in Fig. 7(a). Noting that in [19] the rotated transition cube could not cause so large increase of touching area on the cylindrical surface of TSV, but it brings more speedup to the FRW algorithm. The reason of this is related to how frequently the rotated transition cube is used. For the test cases in this paper, only when the current position of random walk is near a nonaligned side face of conductor the rotated transition cube can be used. However, in each test case the sum of area of nonaligned side faces only counts for a small portion of the total surface area of conductors. As for the TSV case in [19], there are very large and tall cylindrical surfaces. It is relatively often that the current position is near a cylindrical surface. So, the strategy of rotating the transition cube is more frequently used, resulting in larger speedup in [19] than what we have seen in this paper. For a structure with more non-Manhattan conductors and each with larger nonaligned side faces, the proposed FRW algorithm using rotated transition cubes would show more speedup to the FRW algorithm only using Manhattan transition cubes.

It should be pointed out that in the simulation of structures in analog/RF circuit, package or FPD design, the coupling capacitances are sometimes needed. Although the FRW-based methods cost more runtime for calculating a coupling capacitance to the same accuracy as the self-capacitance, it does not mean that they will lose the advantages over the deterministic methods. In [11] and [19], we have shown that while attaining good accuracy on some major coupling capacitances the FRW-based methods are still much faster than the fast BEM solvers. This advantage of runtime becomes more prominent in the situation where a large-scale structure is simulated. On the other hand, it is also not free to make the deterministic method achieving high accuracy on coupling capacitance. As shown in [19], the demand of accurate coupling capacitance usually means denser or more careful panel discretization, which causes the increase of runtime or is just difficult to achieve. On the contrary, the FRW-based method is a discretization-free and embarrassingly parallel method. So, it is more stable and easier to attain good accuracy of coupling capacitance.

V. CONCLUSION

Efficient techniques are proposed to handle the non-Manhattan conductors in the FRW-based capacitance extraction. The proposed techniques enable generating the Gaussian surface and constructing the transition cubes for the structure including non-Manhattan conductors. By modifying the domination judgment, the space management based on candidate list is extended for the non-Manhattan conductor structure, and brings large acceleration to the capacitance extraction. The strategy of using rotated transition cube is also investigated, with corresponding space management technique proposed. With these techniques, an FRW method for the capacitance extraction of non-Manhattan conductor structure has been developed. The method is advantageous for handling large IC, package or FPD structures with non-Manhattan conductors.

The proposed techniques and the related test cases will be added to the future version of RWCap program, which will be shared on the website of the authors.

VI. ACKNOWLEDGMENT

The authors would like to thank all the insightful comments from the reviewers.

REFERENCES

[1] W. Yu and X. Wang, *Advanced Field-Solver Techniques for RC Extraction of Integrated Circuits*. Heidelberg, Germany: Springer, 2014.
[2] M. Takagi *et al.*, "Layout and reticle verification for FPD," in *Proc. SPIE,* vol. 8441, Yokohama, Japan, 2012, pp. 1–4.
[3] A. N. Bhoj, R. V. Joshi, and N. K. Jha, "3-D-TCAD-based parasitic capacitance extraction for emerging multigate devices and circuits," *IEEE Trans. Very Large Scale Integr. (VLSI) Syst.*, vol. 21, no. 11, pp. 2094–2105, Nov. 2013.
[4] K. Nabors and J. White, "FastCap: A multipole accelerated 3-D capacitance extraction program," *IEEE Trans. Comput.-Aided Design Integr. Circuits Syst.*, vol. 10, no. 11, pp. 1447–1459, Nov. 1991.
[5] W. Yu and Z. Wang, "Enhanced QMM-BEM solver for three-dimensional multiple-dielectric capacitance extraction within the finite domain," *IEEE Trans. Microw. Theory Techn.*, vol. 52, no. 2, pp. 560–566, Feb. 2004. [Online]. Available: http://numbda.cs.tsinghua.edu.cn/qbem.htm
[6] S. Yan, V. Sarin, and W. Shi, "Fast 3-D capacitance extraction by inexact factorization and reduction," *IEEE Trans. Comput.-Aided Design Integr. Circuits Syst.*, vol. 25, no. 10, pp. 2282–2286, Oct. 2006.

[7] W. Chai, D. Jiao, and C.-K. Koh, "A direct integral-equation solver of linear complexity for large-scale 3D capacitance and impedance extraction," in *Proc. Design Autom. Conf.*, New York, NY, USA, Jul. 2009, pp. 752–757.

[8] W. Chai and D. Jiao, "Linear-complexity direct and iterative integral equation solvers accelerated by a new rank-minimized H^2-representation for large-scale 3-D interconnect extraction," *IEEE Trans. Microw. Theory Techn.*, vol. 61, no. 8, pp. 2792–2805, Aug. 2013.

[9] G. Chen *et al.*, "ParAFEMCap: A parallel adaptive finite-element method for 3-D VLSI interconnect capacitance extraction," *IEEE Trans. Microw. Theory Techn.*, vol. 60, no. 2, pp. 218–231, Feb. 2012.

[10] Y. Le Coz and R. B. Iverson, "A stochastic algorithm for high speed capacitance extraction in integrated circuits," *Solid-State Electron.*, vol. 35, no. 7, pp. 1005–1012, Jul. 1992.

[11] W. Yu, H. Zhuang, C. Zhang, G. Hu, and Z. Liu, "RWCap: A floating random walk solver for 3-D capacitance extraction of VLSI interconnects," *IEEE Trans. Comput.-Aided Design Integr. Circuits Syst.*, vol. 32, no. 3, pp. 353–366, Mar. 2013. [Online]. Available: http://numbda.cs.tsinghua.edu.cn/rwcap.htm

[12] C. Zhang and W. Yu, "Efficient space management techniques for large-scale interconnect capacitance extraction with floating random walks," *IEEE Trans. Comput.-Aided Design Integr. Circuits Syst.*, vol. 32, no. 10, pp. 1633–1637, Oct. 2013.

[13] W. Yu, "RWCap2: Advanced floating random walk solver for the capacitance extraction of VLSI interconnects," in *Proc. ASICON*, Shenzhen, China, Oct. 2013, pp. 1–4.

[14] C. Zhang and W. Yu, "Efficient techniques for the capacitance extraction of chip-scale VLSI interconnects using floating random walk algorithm," in *Proc. ASP-DAC*, Singapore, Jan. 2014, pp. 756–761.

[15] T. A. El-Moselhy, I. M. Elfadel, and L. Daniel, "A hierarchical floating random walk algorithm for fabric-aware 3-D capacitance extraction," in *Proc. ICCAD*, San Jose, CA, USA, Nov. 2009, pp. 752–758.

[16] A. Brambilla and P. Maffezzoni, "A statistical algorithm for 3-D capacitance extraction," *IEEE Microw. Guided Wave Lett.*, vol. 10, no. 8, pp. 304–306, Aug. 2000.

[17] N. Bansal, "Randomized algorithms for capacitance estimation," Dept. Comput. Sci. Eng., Indian Inst. Technol. Bombay, Mumbai, India, Tech. Rep., Apr. 1999.

[18] F. Bernal, J. A. Acebron, and I. Anjam, "A stochastic algorithm based on fast marching for automatic capacitance extraction in non-Manhattan geometries," *SIAM J. Imag. Sci.*, vol. 7, no. 4, pp. 2657–2674, 2014.

[19] C. Zhang, W. Yu, Q. Wang, and Y. Shi, "Fast random walk based capacitance extraction for the 3-D IC structures with cylindrical inter-tier-vias," *IEEE Trans. Comput.-Aided Design Integr. Circuits Syst.*, vol. 34, no. 12, pp. 1977–1990, Dec. 2015.

[20] G. Rollins. (Jul. 2010). "Rapid3D 20X Performance Improvement," [Online]. Available: http://www.synopsys.com/Community/UniversityProgram/Pages/Presentations.aspx

[21] K. Li, "Energy efficient scheduling of parallel tasks on multiprocessor computers," *J. Supercomput.*, vol. 60, no. 2, pp. 223–247, Mar. 2012.

[22] D. Xiang and W. Luo, "An efficient adaptive deadlock-free routing algorithm for torus networks," *IEEE Trans. Parallel Distrib. Syst.*, vol. 23, no. 5, pp. 800–808, May 2012.

[23] *QuickCap and QuickCap NX Technology Guide*, Magma Inc., San Diego, CA, USA, 2009.

[24] M. Mascagni and C.-O. Hwang, "ϵ-shell error analysis for 'walk on spheres' algorithms," *Math. Comput. Sim.*, vol. 63, no. 2, pp. 93–104, 2003.

[25] W. H. Press, S. A. Teukolsky, W. T. Vetterling, and B. P. Flannery, *Numerical Recipes in C*, 2nd ed. Cambridge, U.K.: Cambridge Univ. Press, 1992.

[26] B. Zhou and D. Jiao, "Linear-complexity direct finite element solver accelerated for many right hand sides," in *Proc. IEEE Int. Symp. Antennas Propag.*, Memphis, TN, USA, Jul. 2014, pp. 1383–1384.

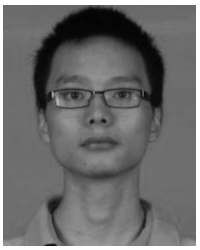

Zhezhao Xu received the B.S. degree in electronic science and technology from the Huazhong University of Science and Technology, Wuhan, China, in 2014. He is currently pursuing the M.S. degree in computer science with Tsinghua University, Beijing, China.

His current research interests include capacitance extraction field solver, parallel computing, and machine learning.

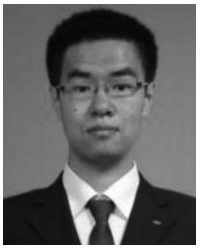

Chao Zhang received the B.S. and M.S. degrees in computer science from Tsinghua University, Beijing, China, in 2012 and 2015, respectively.

He is currently with Hulu Inc., Beijing, China, researching on video playback experience. His research interests include computing algorithm and interconnect capacitance extraction.

Mr. Zhang was a recipient of the Outstanding M.S. Award from Tsinghua University, in 2015, and the Best Paper Award from the Design, Automation and Testing in Europe Conference, in 2016.

Wenjian Yu (S'01–M'04–SM'10) received the B.S. and Ph.D. degrees in computer science from Tsinghua University, Beijing, China, in 1999 and 2003, respectively.

He joined Tsinghua University, Beijing, China, in 2003, where he is an Associate Professor with the Department of Computer Science and Technology. He was a Visiting Scholar with the Department of Computer Science and Engineering, University of California at San Diego, San Diego, CA, USA, twice during the period from 2005 to 2008. He has authored two books and over 130 papers in refereed journals and conferences. His current research interests include physical-level modeling and simulation techniques for IC design, electromagnetic field solvers, and a broad range of numerical methods.

Dr. Yu was a recipient of the Distinguished Ph.D. Award from Tsinghua University in 2003, the Excellent Young Scholar Award from the National Science Foundation of China in 2014, and the Best Paper Award from the Design, Automation and Testing in Europe Conference in 2016.